Polymerization mechanism of nitrogen-containing heteroaromatic compound under high-pressure and high-temperature conditions

Ayako Shinozaki[a]*, Koichi Mimura[b], Tamihito Nishida[b], George D. Cody[c]

[a]Faculty of Science, Hokkaido University, N10 W8, Kita-ku, Sapporo, Hokkaido 060-0810, Japan

[b]Department of Earth and Planetary Sciences, Graduate School of Environmental Studies, Nagoya University, Nagoya 464-8601, Japan

[c]Earth and Planets Laboratory, Carnegie Institution of Washington, 5251 Broad Branch Road, NW, Washington, DC 20015, USA

* Corresponding author: Ayako Shinozaki

E-mail: shinozaki.aya@sci.hokudai.ac.jp

Abstract

Hydrogenated carbon nitride is synthesized by polymerization of 1,5-naphthyridine, a nitrogen-containing heteroaromatic compound, under high-pressure and high-temperature conditions. The polymerization progressed significantly at temperatures above 573 K at 0.5 GPa and above 623 K at 1.5GPa. The reaction temperature was relatively lower than that observed for pure naphthalene suggesting the reaction temperature is considerably lowered when nitrogen atoms exist in the aromatic ring structure. The polymerization reaction largely progresses without significant change of N/C ratio. Three types of dimerization are identified; naphthylation, exact dimerization, and dimerization with hydrogenation as determined from the GC/MS analysis of soluble products. IR spectra suggest hydrogenation products were likely to be formed with sp^3 carbon and NH bonding. ^{13}C ssNMR reveals that the sp^3/sp^2 ratio is 0.14 in both the insoluble solids synthesized at 0.5 and 1.5 GPa. Not only the dimers but also soluble heavier oligomers and insoluble polymers formed through more extensive polymerization. The major reaction mechanism of 1,5-Nap was common to both the 0.5 and 1.5 GPa experiments, although the required reaction temperature increased with increasing pressure and aromatic rings preferentially remained at the higher pressure.

Introduction

Carbon nitride materials have attracted attention due to their potential applications in metal-free photocatalysis [1-2] and photodegradation [3]. Various crystalline polymorphs of C_3N_4 were reported and theoretical studies pointed out that the hardness of some C_3N_4 phases were comparable or even higher than that of diamond [4-8]. Amorphous carbon nitrides have also been synthesized by chemical vapor deposition (CVD) and physical vapor deposition (PVD) techniques [9]. To synthesize and characterize nitrogen-doped carbon materials, it is important to evaluate N/C ratios, sp^3/sp^2 ratios, and behavior of hydrogen atoms during the synthesis which are generally retained in nitrogen-doped carbon materials as essential components of their structures [10]. The application of high-pressure and high-temperature (HPHT) conditions is considered a useful technique for the synthesis of carbon nitride materials as well as CVD and PVD techniques [11]. The crystal structures and bonding of carbon nitride materials have been investigated above 100 GPa and/or above a few thousand kelvin using laser heated diamond anvil cells [12-14], although it was difficult in these studies to reveal the mechanism of the chemical reaction because controlling the heating temperature is difficult and analytical methods are limited due to the extremely small sample size in diamond anvil cell devices. Several HPHT experiments using large-volume presses, such as piston-cylinder apparatus, belt-type press, and multi-anvil press have also been performed. Various analytical methods such as X-ray diffraction (XRD)

measurements, Raman and infrared (IR) spectra, X-ray photoelectron spectroscopy (XPS), and transmission electron microscope (TEM) with electron energy loss spectroscopy (EELS) have been used to evaluate crystallinity, chemical compositions, and bonding of the reaction products [11, 15-19]. It has been reported that the N/C ratio of carbon-nitride materials decreases with increasing temperature, in the case where synthesis focused on 1,2,4-triazole ($C_2N_3H_3$) [19] and melamine ($C_3N_6H_6$) [17]. Graphitic C_3N_4 decomposed into diamond and probably N_2 above 1073-1173 K at 22-25 GPa [18]. However, details of the reaction mechanism remain unclear.

The pressure-induced polymerization mechanism of various aromatic compounds including nitrogen-containing heteroaromatic compounds have also been studied [20-25] and it was generally concluded that the decrease of the intermolecular distances with increasing pressure resulted in polymerization [26-27]. Polymerized products were obtained after compression above 20 GPa at room temperature and some products were shown to exist as an amorphous solid phase containing considerable sp^3 carbon [22-23, 25]. One-dimensional sp^3 carbon nitride nanothreads have been shown to form from slow compression/decompression of pyridine (C_5H_5N) [28-29] and aniline ($C_6H_5NH_2$) [30] to around 20 GPa as well as carbon nanothreads formed from the high pressure polymerization of benzene (C_6H_6) [31-32]. The atomic N/C ratio of the carbon nitride nanothreads was not considerably changed from that of the starting material while significant conversion from sp^2 to sp^3 bonding occurred during the reaction [28]. Diffraction measurements suggested a

polytwistane structure for the carbon nitride nanothread derived from a [4+2] Diels-Alder cycloaddition reaction [29].

Applying HPHT conditions to aromatic compounds potentially induces complex reactions because H-elimination and polycondensation can be induced by temperature, noting that it is clear that oligomerization/polymerization are likely to be induced by pressure. Oligomerization of aromatic hydrocarbons has been observed at 500–773 K at ambient pressure and at 3.5 GPa, and 773–973 K at 7 GPa [33-34]. Oligomerization with dehydrogenation and new C-C bond(s) formation between the aromatic rings were reported by using mass spectrometry of the reaction products [33]. Shock experiments on benzene, naphthalene and other PAHs showed that amorphous carbon, hydrogen/hydrocarbon gases, and oligomers were formed at shock pressures and temperatures above around 10 GPa and 800 K [35-36]. In shock experiments of naphthalene, optically dark products of amorphous carbon were predominantly observed. In addition, various methylation, phenylation, and naphthylation products were formed by radical reactions [36]. HPHT experiments revealed that polymerization of pyridine proceeds at approximately 8 GPa and 750–800 K, a reaction temperature that was distinctly lower than that of benzene polymerization [37]. However, details regarding the reaction mechanism and the specific role of nitrogen during the course of the reaction has not been resolved.

Naphthyridines ($C_8H_6N_2$) consist of two fused aromatic rings like naphthalene, but

where two of the CH groups are replaced with nitrogen atoms. There are several isomers that differ in the position of nitrogen atoms in the aromatic rings. Pressure-induced irreversible reaction of 2,3-naphthyridine (hereafter 2,3-Nap) and 1,5-naphthyridine (hereafter, 1,5-Nap) to form amorphous solids were observed at around 16-18 GPa at room temperature at pressures not remarkably different for the polymerization of naphthalene [25]. The recovered amorphous products contained a considerable amount of nitrogen bonded to both sp^3 and sp^2 carbons [25]. The temperature-induced chemical reaction of 2,3-Nap was reported at >523 K at 0.5 and 1.0 GPa, and >548 K at 1.5 GPa [38]. The reaction products were investigated by using gas chromatograph-mass spectrometry (GC/MS) and matrix-assisted laser desorption/ionization (MALDI) Time of Flight (TOF) mass spectrometry (MS), and cleavage of the aromatic ring and release of nitrogen atoms with the formation of o-xylene and o-tolunitrile were indicated. In addition, the decomposed products reacted with the remaining 2,3-Nap to form larger oligomers. The N-N bond in the aromatic ring accelerated reactions to decompose the molecule and to oligomerize at lower temperatures than those typically reported for pure aromatic hydrocarbon oligomerization reactions. In the 1,5-Nap molecule, nitrogen atoms are located in separate aromatic rings (Figure 1) and the molecule possesses a center of symmetry and belongs to the point group C_{2h} [39] in contrast to 2,3-Nap. In this study, polymerization of 1,5-Nap under HPHT conditions was experimentally investigated at temperatures between 473-623 K and at pressures of 0.5 GPa and

1.5 GPa. Complex reaction products including soluble dimers and heavier oligomers, and insoluble hydrogenated carbon nitride were identified and were evaluated analytically to reveal the details of the reaction process and nitrogen behavior during the reaction.

Experimental

1,5-naphthyridine ($C_8H_6N_2$, Tokyo Chemical Industry Co. LTD., purity >98 %) and naphthalene ($C_{10}H_8$, Sigma-Aldrich, purity >99.7%) for about 10-20 mg was used as the initial material for the HPHT experiments. A gold sample capsule with 4 mm outer diameter was cleaned with acetone or dichloromethane and heated in an oven at 450 °C for 4 h prior to encapsulating the sample to remove organic contaminants. The sample was welded shut following which the capsule was pressurized using a piston-cylinder apparatus equipped with a hydraulic press and tungsten carbide rams and compression ring. A cylinder with 4 mm inner diameter was used without a pressure medium. The sample was first compressed to the target pressure at room temperature and then heated using a band-type external heater surrounding the cylinder. The temperature was measured using a K-type thermocouple attached to the top of the cylinder. The details of the apparatus were described in a previous study [38]. The reaction time for all experiments was fixed at four hours.

The samples after the HPHT experiments were recovered from the capsules in distilled dichloromethane solvent to prevent the reaction products from escaping. The solution was initially

109 filtered by carbon-free glass filter to extract soluble products from insoluble products. The carbon,
110 nitrogen and hydrogen contents of the reaction products were analyzed using an elemental
111 analyzer (Vario EL cube; Elementar Analysensysteme GmbH) for the soluble samples after
112 evaporating the solvent and for the insoluble samples. IR spectra of the soluble reaction product
113 were obtained in solid-state after drying in a vacuum desiccator ensuring that the solvent and the
114 stating material were removed. Both soluble and the insoluble products were pelletized with KBr
115 plates and IR absorption spectra in the mid-IR region were measured. A Fourier transform IR
116 spectrometer (FT-IR: FTIR-6100/IRT-5000; Jasco) was used equipped with a globar source, a
117 KBr beam splitter, and a liquid nitrogen cooled mercury cadmium telluride (MCT) detector. The
118 typical aperture size was 50 × 50 μm. The wavenumber resolution was set to 4 cm^{-1}.
119 For soluble products, mass spectrometry was performed using a GC/MS (JMS-K9; JEOL
120 Co.) equipped with a 30 m × 0.25 mm I.D. capillary column, with a 0.25 μm layer of stationary
121 phase (HP-5, Agilent Technology Co.). The GC column temperature was programmed as in our
122 previous studies [38, 40]. A GC-flame ionization detector (GC/FID, GC-2014; Shimadzu) equipped
123 with an HP-5 capillary column was used for quantitative analysis of the remaining 1,5-Nap and
124 the reaction products. The GC column temperature was programmed as in the GC/MS
125 measurements. Methyl laurate ($C_{13}H_{26}O_2$), methyl stearate ($C_{19}H_{38}O_2$), and methyl triacontanate
126 ($C_{31}H_{62}O_2$) were used as internal standards for GC/FID and GC/MS analyses. The mass spectra

of the reaction products were also analyzed using a MALDI-TOF/MS instrument (Ultraflex-III and Autoflex-III, Bruker), with an α-cyano-4-hydroxycinnamic acid (α-CHCA) matrix.

Solid-state ^{13}C nuclear magnetic resonance (ssNMR) spectroscopy of the insoluble products were performed with a Varian-Chemagnetic Infinity 300 Nuclear Magnetic Resonance spectrometer. The resonance frequency of ^{13}C was 75 MHz. The insoluble products were loaded into a zirconia oxide capsule (outside diameter of φ5 mm for ^{13}C NMR) with boron nitride inserts to position the small sample in the middle of the RF coil. For the ^{13}C NMR measurement, a ^{1}H-^{13}C cross polarization with magic angle spinning (CP-MAS) experiment was conducted. The MAS frequencies were 12 kHz. Variable amplitude cross polarization (VACP) was used to ramp up the RF power on the ^{13}C channel during the CP contact time. The ^{1}H 90º excitation pulse length was 4 μs. A variable contact time (form 1 to 12 ms) CPMAS experiment was performed in order to optimize signal and minimize distortion due to variation in C-H distances, the optimum ^{1}H-^{13}C contact time for maximum signal for both sp^2 and sp^3 carbon was found to be 4.5 ms. In order to achieve adequate signal to noise the number of acquisitions was 80,000×4times with a recycle delay of 1s, thus each sample spectrum required ca. 4 days of signal acquisition. The chemical shift of ^{13}C NMR spectra were calibrated by solid hexamethylbenzene that was referenced to tetramethylsilane (TMS).

Results

1. P-T conditions of the chemical reaction.

The HPHT experiments with 1,5-Nap performed at 0.5 and 1.5 GPa, and at temperatures ranging from 473 to 623 K are listed in Table 1. In addition, a HPHT experiment of naphthalene at 1.5 GPa and 623 K was performed for comparison. During the HPHT experiments of 1,5-Nap at 0.5 GPa, the stroke of the piston discontinuously increased when the temperature reached around 533 K, implying melting of 1,5-Nap. In contrast, such a discontinuity was not observed during the heating at 1.5 GPa up to 623 K, suggesting 1,5-Nap remained as a solid at 1.5 GPa.

Figure 2 and table 1 show the remaining percentage of 1,5-Nap as determined by GC/FID analysis of the recovered samples. At 0.5 GPa, the percentage of recovered 1,5-Nap decreased to around 75 %, initial, after heating at 523 K and 548 K. In addition, the solution of the recovered samples changed to yellow, while the solution of starting material was transparent. These results indicate that the chemical reaction starts around that temperature to form soluble reaction products. After heating at >573 K, the remaining 1,5-Nap decreased to < 6 %, and a black insoluble product was observed in a brown solution indicating that the chemical reaction progressed significantly to form both soluble and insoluble products. 1,5-Nap is nearly absent after heating at 598 and 623 K, and insoluble solid product formed but the solution of these samples was transparent suggesting most of the soluble reaction products were now in the insoluble solid phase. At a pressure of 1.5 GPa, most of the 1,5-Nap still remained unreacted after heating at <573 K. The

163 remaining 1,5-Nap decreased to approximately 60 % after heating at 598 K and dropped further
164 to ~ 5 % after heating at 623 K with both soluble and insoluble product clearly evident. The results
165 indicate the thermal onset of chemical reaction of 1,5-Nap was above 523 K at 0.5 GPa, and above
166 548 K at 1.5 GPa, namely the required reaction temperature increases with increasing pressure.
167 In contrast, most of naphthalene was recovered after heating at 1.5 GPa at 623 K and reaction
168 products were not detected.

169 **2. The soluble products**

170 The elemental analysis of the soluble product from 1.5 GPa, 623 K showed N/C and H/C ratio
171 as 0.242 ± 0.002 and 0.762 ± 0.046, respectively which was nearly equal to that of the starting
172 material (N/C = 0.249 ± 0.001, H/C = 0.720 ± 0.054) suggesting nitrogen and hydrogen atoms
173 are very largely retained in the reaction products. FT-IR analysis reveals some IR peaks in the
174 soluble products (Figure 3a, b) that are comparable in frequency with those observed from the
175 starting material [39]. For example, the C-H bending modes at around 820, 840, 1110, 1190, 1220
176 cm^{-1}, ring stretching modes at around 1300, 1400, 1490, and 1590 cm^{-1}, C-H stretching modes at
177 around 3000-3100 cm^{-1} were obtained from the soluble products while the width of the peaks
178 became broader than those in the IR spectrum of the initial material. In contrast, a significant
179 decrease in the intensity of the skeletal deformation mode absorbance at around 1018 cm^{-1} was
180 observed. It is clear that aromatic rings remain even in the reaction products, although as they are

181 now polymerized. In addition, new peaks were detected in the spectra of the reaction products.
182 The peaks observed at 1350 and 1450 cm^{-1} are interpreted to be sp^3 C-H bending modes, and the
183 peaks at 2850, 2930, and 2960 cm^{-1} are fundamental C-H stretching modes associated with sp^3
184 carbon [41-42]. The peaks appeared at around 730 and 790 cm^{-1} are assigned to N-H wagging modes
185 and a new peak near 1620 cm^{-1} is likely a N-H bending mode. Finally, the broad peak spanning
186 3230 and 3320 cm^{-1} is likely due to fundamental N-H stretching modes [41].

187 A considerable number of dimers were detected by GC/MS and GC/FID analysis of the
188 soluble reaction products. The mass number and possible molecular structure of the reaction
189 products were estimated by the clearly identified molecular ions in all of the mass spectra. Figure
190 4a, b shows representative total ion chromatogram (TIC) at 1.5 GPa, 623 K and 0.5 GPa 573 K.
191 Four isomers of $[M]^{\bullet+}$ = 258 were detected (Figure S1a), which were likely to be formed by
192 naphthylation, defined as dimerization with dehydrogenation. Products of $[M]^{\bullet+}$ = 260 (Figure
193 S1b) were also detected, with a molecular ion mass consistent with exactly twice of that of 1,5-
194 Nap indicating those products formed by dimerization without release of any atoms, e.g.,
195 hydrogen. Several products which has $[M]^{\bullet+}$ = 262 and 264 were detected (Figure S1c and S1d,
196 respectively), which interpreted to be dimers of 1,5-Nap with hydrogeneration of 2H's and 4H's,
197 respectively. Hence, the major reaction products of dimers are classified as three types,
198 naphthylation (2M-2H), exact dimerization (2M), and hydrogenation dimerization (2M+2H,

2M+4H). Reaction products with $[M]^{\bullet+}$ = 386, 388 and 392 were also detected, which are likely trimers formed by combination of these three types of reaction. The hydrogenation of 1,5-Nap was also suggested by the presence of a product with a molecular ion $[M]^{\bullet+}$ = 134 (Figure S2a) detected in the recovered samples from >523 K, at 0.5 and 1.5 GPa (Table S1). In addition, minor peaks with $[M]^{\bullet+}$ = 236, 250 were also detected. These are interpreted to form by the partial ring opening with release of two or one carbon atom(s) from the dimer. Minor peaks with $[M]^{\bullet+}$ = 276, 278 were also detected, which could be methylation products of $[M]^{\bullet+}$ = 262, 264. Methylation might occur when the released carbon by the partial ring opening dimers reacts with simple dimers.

The approximate molar yields of the several dimers were roughly quantified using the peak area of the chromatogram relative to that of an internal standard (methyl stearate) measured by GC/FID. The response factor of 1,1'-biphenyl was used for the quantification, whose structure was regarded as being similar to that of the naphthylation dimers. Table S1, Figure 5a and 5b shows the molar yield of the representative reaction products, in which sum of four isomers of $[M]^{\bullet+}$ = 258, three isomers of $[M]^{\bullet+}$ = 260, seven isomers of $[M]^{\bullet+}$ = 262, five isomers of $[M]^{\bullet+}$ = 264, five isomers of $[M]^{\bullet+}$ = 276, 278, and one each for products $[M]^{\bullet+}$ = 236, 250 were included. The dimers were detected above 523 K at 0.5 GPa, the total molar yields increasing with increasing temperature up to 548 K. With increasing temperature above 573 K the total molar yields of dimer decreases relative to that of lower temperatures. At 1.5 GPa, the dimers were

detectable above 548 K and the total molar yields increase with increasing temperature up to 623 K. Figure 5c and 5d presents the relative ratio of the reaction products from 523-573 K at 0.5 GPa and from 598, 623 K at 1.5 GPa, respectively, in which total molar yields of the dimers excess 1 %. At 0.5 GPa, relative concentration of $[M]^{\bullet+}$ = 258 decreased with increasing temperature, while those of $[M]^{\bullet+}$ = 262, 264 increased. In contrast, the proportion of $[M]^{\bullet+}$ = 258 slightly increased and $[M]^{\bullet+}$ = 264 decreased with increasing temperature to 623 K at 1.5 GPa. These results suggest that hydrogenation occurs more frequently at lower pressure. Molecules with $[M]^{\bullet+}$ = 236, 250 and $[M]^{\bullet+}$ = 276, 278, which are products interpreted to form with ring opening, were detected only 573, 598 K at 0.5 GPa, and 598, 623 K at 1.5 GPa (table S1) and the relative percentage is much less than that of the products with $[M]^{\bullet+}$ = 258, 260, 262, and 264. The ring-opening reaction is, therefore, considered to be a minor reaction. The proportion of sum of $[M]^{\bullet+}$ = 236, 250, 276, and 278 are on the order of 8 % at 0.5 GPa 573 K, where this sum is on the order of 1 % at 1.5 GPa 623 K even though the remaining percentage of 1,5-Nap were similar so the reaction progress was in both cases similar in rate. These results suggest that the ring-opening reactions preferentially occur at lower pressure.

Figure 6 presents a representative MALDI-TOF/MS spectrum of the sample recovered from 1.5 GPa, 573 K and the inset shows enlarged view of ions in the range of *m/z* = 250-290. Intense peaks of *m/z* = 259-269 were detected, and the molar weight was comparable that of the

235 dimers of 1,5-Nap detected by the GC/MS, while some of the peaks in MALDI-TOF spectra were
236 likely $[M+H]^{\bullet+}$ ions, a common feature of MALDI-TOF/MS. In addition, peaks of m/z = 275-279
237 were detected. These peaks might be $[M+H]^{\bullet+}$ ions of methylation products of the 1,5-Nap dimers.
238 The series of clusters appear periodically approximately 130 mass units apart which was
239 comparable to the molar weight of the starting material. Molecular clusters are observed up to
240 masses in excess of *m/z* = 2000. Each cluster are reasonably interpreted to represent dimers,
241 trimers, and higher oligomers up to N=15.

242 **3. The insoluble hydrogenated carbon nitride polymer**

243 A considerable amount of insoluble hydrogenated carbon nitride polymer was obtained from the
244 recovered samples from >573 K at 0.5 GPa and >598 K at 1.5 GPa (as discussed above). The
245 elemental analysis of the insoluble products from 1.5 GPa at 623 K shows that the N/C = 0.2476
246 ± 0.0003. The N/C ratio is comparable with that observed in the starting material indicating that
247 selective release of nitrogen had scarcely occurred. H/C ratio of the insoluble products was 0.653
248 ± 0.015, which is lower than that of the initial material and the soluble products and indicates a
249 loss of ca. 13 % hydrogen. Figure 3 c, d presents the IR spectra of the insoluble materials from
250 1.5 GPa at 623 K and 0.5 GPa at 623 K, respectively. Many of the IR peaks appears at
251 wavenumbers similar to those in the soluble product (Fig. 3b) although the peak widths and
252 relative intensities are slightly different. The peak absorbance between 1100-1600 cm^{-1} is larger

253 than from soluble product suggesting the formation of a broad peak in this region underlying the
254 sharper vibrational peaks. These results suggest that the soluble and insoluble products are both
255 formed in a series of polymerization reactions, but the insoluble products are likely formed from
256 additional polymerization reactions beyond that which formed the oligomerized soluble products.
257 This is evident as H/C ratio of the insoluble products is lower than that of the soluble products by
258 13 %, implying that polymerization with dehydrogenation account for large percentage of the
259 solid products.

260 We measured ^{13}C ssNMR spectra of the starting material and the insoluble reaction
261 products obtained from 0.5 GPa, 623 K, and 1.5 GPa, 623 K. A spectrum of pure 1,5-Nap was
262 acquired but suffered from very long spin-lattice (T_1) relaxation times and poor cross polarization
263 dynamics (i.e., long T_{CH} and short $T_{1\rho}$) resulting in a frustratingly low S/N ratio. Nevertheless,
264 three of the four magnetically inequivalent carbon nuclei are clearly observed as very sharp peaks
265 at 124.5 (carbons 3 & 7), 137.5 (carbons 4 & 8) and 151.5 ppm (carbons 2 & 6) were detected in
266 the ^{13}C ssNMR spectrum of pure 1,5-Nap, all of which are assignable as sp^2 carbon (Figure S3).
267 Interestingly, we could not detect the bridgehead carbon atoms (9 & 10) predicted to be at ~ 144
268 ppm, this is likely due to the lack of protonation and poor ^{1}H-^{13}C cross polarization efficiency.
269 The peak areas of the three peaks that are observed are essentially equal (given the low S/N) as
270 expected (the 9 & 10 bridgehead carbon atoms would be expected to be equal in intensity to the

271 other three carbon types).

272 In the ^{13}C ssNMR spectra of the insoluble products, both sp^3 (major in abundance) and
273 sp^2 carbon (minor in abundance) are detected (Figure 7). The sp^3/sp^2 ratio was determined to be
274 0.14 based on the peak areas in the ^{13}C ssNMR spectra; where a pressure dependence on this ratio
275 was not observed. The sp^2 region of the ^{13}C ssNMR spectra could be adequately fit by four broad
276 peaks at frequencies around 122, 136, 142, and 151 ppm (Figure S4a and S4c) that likely
277 correspond to the 3 & 7, 4 & 8, 9 & 10, and 2 & 6 carbon atoms of the 1,5-Nap precursor,
278 respectively. Variable contact time experiments show that the peak at 142 ppm has a cross
279 polarization rate time constant (T_{CH}) of 950 μs, whereas the 122 pm peak has a T_{CH} of 540 μs; the
280 larger value of T_{CH} for the 142 ppm peaks is consistent with the assignment of bridge head carbon
281 that is more distant from protons. Whereas the four magnetically inequivalent carbon types in 1,5-
282 Nap "monomer" would be expected at equal intensities, integration of the four peaks that
283 dominate the sp^2 carbon region for the insoluble solids reveals differences in the percent
284 contribution of certain carbons to the total sp^2 region. For example, 0.5 GPa solids, peaks at 151
285 and 136 ppm (likely corresponding to the 2 & 6 and 4 & 8 carbons in the 1,5-Nap "monomer")
286 are considerably weaker than that of the 142 and 122 ppm peaks (likely corresponding to the 9 &
287 10, bridge head, carbons and the 3 & 7 carbons) (Table S2a). In the case of the 1.5 GPa solids,
288 peak intensity at 136 ppm (the 4 & 8 carbon atoms) is significantly weaker than the other three

289 peaks (Table S2b). Such selective reductions in intensity of certain carbon peaks may signify
290 which of the initial 1,5-Nap carbon atoms are involved in the pressure and temperature induced
291 formation of polymeric linkages.

292 The peaks corresponding to sp^3 carbon (0 to 60 ppm) can be adequately fit with five and
293 four peaks (Figure S4b, d, respectively). The relatively intense peaks at ~ 23, 30, and 38 ppm are
294 consistent with aliphatic carbon (largely CH_3, CH_2 and CH groups, respectively) where the CH_2
295 groups are predominant in both samples formed at 0.5 GPa and 1.5 GPa. Higher frequency weak
296 peaks at 45, and 54 ppm are consistent with sp^3 carbon bonded to -NH and -N, respectively [41].
297 These peaks are present in the sample from 1.5 GPa (Figure S4b), although, but reduced in
298 intensity in the 0.5 GPa experimental products (Figure S4d) suggesting that nitrogen atoms are
299 more associated with sp^2 carbon in the lower pressure solid products. A shoulder peak at 13 ppm
300 was observed only from the spectrum from 0.5 GPa, which could be ascribed to CH_3 groups [41]. It
301 is suggested in these two ^{13}C ssNMR spectra that methyl groups intensity is slightly enhanced in
302 the lower pressure solid products.

303 **Discussion**

304 The chemical reaction of 1,5-Nap proceeds significantly above 573 K at 0.5 GPa and above 623
305 K at 1.5GPa and soluble reaction products revealing oligomerization are readily obtained from
306 the samples recovered from >523 K at 0.5 GPa and >548 K at 1.5 GPa. The insoluble

307 hydrogenated carbon nitride polymer was synthesized from >573 K, at 0.5 GPa, and >598 K at
308 1.5GPa. N/C ratio of the reaction products of both soluble and insoluble products were quite
309 similar with that of 1,5-Nap, indicating that release of nitrogen atoms with chemical reaction was
310 limited with the solids forming reaction in the present temperature ranges and that the nitrogen
311 atom was contained in an aromatic ring and connected only with carbon. In contrast, nitrogen
312 atoms are selectively released from aromatic rings with the oligomerization when two nitrogen
313 atoms were localized in one aromatic ring forming a N-N bonding as in 2,3-Nap [38]. In case of 2,3-
314 Nap, the N-N covalent bond is easily dissociated under high temperature and the aromatic ring
315 was subjected to both nitrogen and carbon opening reactions.

316 The dimers of the reaction products which were detected by the GC/MS analysis of the
317 soluble products clarified into three types of dimerization products, that is naphthylation (2M-
318 2H), exact dimerization (2M), and dimerization with hydrogenation (2M+2H, 2M+4H) products.
319 In contrast, naphthalene dimers were not detected from 1.5 GPa and 623 K in this study and
320 oligomerization with naphthylation of naphthalene was reported at 773 K, 7 GPa and at 820 K,
321 ambient pressure in the previous studies [33-34]. These results indicate that reaction temperature for
322 polymerization was lowered by existence of nitrogen even though naphthylation reactions can
323 occur in both naphthalene and in 1,5-Nap. In case of oligomerization of naphthalene, dimerization
324 with release of 2H and 4H, with formation of condensation products were observed at ambient

pressure and high pressure [33, 43-44]. It was pointed out that the cleavage of a carbon-hydrogen bond to produce a highly reactive free radical can initiate polymerization at ambient pressure [43-44]. In contrast, dimerization products with release of 4H were not detected in the present study of 1,5-Nap. Exact dimerization (2M), and dimerization with hydrogenation (2M+2H, 2M+4H) were formed by the 1,5-Nap reaction while these products were not observed in the naphthalene oligomerization [33, 43-44]. The dimerization reaction for 1,5-Nap is, therefore, somewhat different than that observed in case of naphthalene oligomerization. Exact molecular structures are not unambiguously revealed from the mass spectrometry, although the IR spectra (Fig 3) of the soluble reaction products suggested both modest amounts of sp^3carbon and NH functional groups are formed during the reaction. [2+2] and [4+2] Diels-Alder cycloaddition reactions are the likely initiation pathways to form the various dimers including both dehydration and hydrogenation dimers (Figure 8a). The products of $[M]^{\bullet+}$ = 262, 264 would be formed from hydrogenation of the exact dimerization products. Several isomers of the dimers are found so that further studies through theoretical analysis is required to confirm the details of the reaction pathway(s). In case of the pressure-induced reaction of benzene, Diels-Aider reactions are clearly the pathway to form various oligomers [27, 31]. For polymerized benzene, three types of low molecular weight dimerization products are identified, including biphenyl (2M-2H), benzene dimers (2M), and naphthalene (2M-C_2H_4) all formed by the pressure-induced oligomerization of benzene after

343 compression above 13 GPa, room temperature [45]. In contrast, for 1,5-Nap condensed dimers
344 formed with elimination of ethylene were not detected in the reaction products. Elimination of
345 ethylene is evidently limited in the present pressure and temperature ranges. In addition, a
346 hydrogenation product of a molecular ion $[M]^{\bullet+}$ = 134 suggests that hydrogenation without
347 dimerization had also progressed. In the present temperature ranges, hydrogen atoms prefer to
348 remain in the carbon nitride polymer products and even bond with nitrogen atoms. Higher
349 temperatures would be required before large-scale dehydrogenation would occur as has been
350 reported for other aromatic hydrocarbons [33]. Several products formed by ring-opening and
351 methylation were detected, although those quantities were remarkably small compared with that
352 of the three types of dimerization, thus are very minor side reactions.
353 ^{13}C ssNMR spectral analysis of the insoluble products indicate that the sp^3/sp^2 ratio is
354 small, on the order of 0.14. For the purpose of this discussion, consider a proposed "infinite" 1,5-
355 Nap insoluble polymer formed exclusively through 3,4-7,8 [2+2] cycloaddition linkages as shown
356 in Figure 8b; where the corresponding sp^3/sp^2 ratio would be 1.0. This is much higher than what
357 is measured. If 100 % dehydrogenation ($-H_2$) occurred (let's say at the respective 7,4 carbons)
358 yielding a purely "bi-naphthrydine" linked polymer (Figure 8c) the sp^3/sp^2 ratio would be zero.
359 It can be easily shown that if 50 % formation of "bi-naphthridine" linkages yields an sp^3/sp^2 ratio
360 of 0.33. The ^{13}C ssNMR data, therefore, reveal that the polymer contains both the cycloaddition

linkages (Figure 8b) and bi-naphthyridine linkages (Figure 8c) which form by elimination of hydrogen from the decomposition of the cycloaddition linkages in the polymer. Given that the sp^3/sp^2 ratio of the insoluble polymer is measured at 0.14 suggests that around 75 % of the polymer linkages are bi-naphthyridine linkages. The H/C ratio of the insoluble product is 0.65, which is significantly higher than the H/C ratio calculated when the polymer consists of 75 % of the bi-naphthyridine linkages (where H/C would be predicted to be 0.558). The high H/C ratio suggests that CH_2/CH_3 and NH functional groups are also contained in the polymer as is indicated in the IR spectra (Figure 3c, d) and the ^{13}C ssNMR spectra (Figure 7). It is interesting to note that the sp^3/sp^2 ratio of the carbon nitride nanothreads was previously reported to be around 3.5 [28] and in the case of polymer formed from benzene the sp^3/sp^2 ratio is nearly 4.0 (where all of the sp^3 carbon is CH)[31], which is much higher than that in the insoluble material ($sp^3/sp^2 = 0.14$) characterized in this study (where the sp^3 carbon for the 1,5-Nap polymer is predominantly CH_2) [31].

Evidence of polymerization through naphthylation, exact dimerization, and hydrogenation was observed in the recovered samples of both 0.5 and 1.5 GPa. The sp^3/sp^2 ratio as determined through ^{13}C ssNMR of the insoluble products obtained after heating at 0.5 GPa, and 1.5 GPa was nearly the same at 0.14. These results indicate that the major polymerization mechanism(s) is similar at 0.5 GPa and 1.5 GPa, even though the reaction progresses in the liquid phase at 1,5-Nap at 0.5 GPa, and in the solid phase at 1.5 GPa. However, several indications of

379 pressure dependency on the polymerization are suggested. For example, the reaction threshold
380 temperature was changed from 573 K at 0.5 GPa to 623 K at 1.5 GPa. The reaction threshold
381 temperature of benzene is discontinuously changed with the phase state of the starting monomer,
382 especially between liquid and solid phases [46]. In the case of some aromatic compounds, the onset
383 temperatures of the chemical transformation from solid monomers to polymers decrease or are
384 nearly constant with increasing pressure [30, 46-49]. The change of the reaction threshold temperature
385 of 1,5-Nap between 0.5 GPa and 1.5 GPa would be related with the phase state of the stating
386 monomer. Further *in-situ* experiments on structure and phase state relation of 1,5-Nap are
387 necessary for understanding the effect of pressure on the reaction temperature. Quantitative
388 analysis of the dimers suggested that the hydrogenation reactions preferentially progresses at
389 lower pressure. The reaction products related with the ring-opening are also preferentially
390 detected in the lower pressure experiments. Clear differences in the relative abundance of different
391 sp^2 carbon types are observed via ^{13}C ssNMR as a function of pressure and may indicate
392 differences in the types of monomer linkages. Formation of a minor amount of methyl groups
393 observed via ^{13}C NMR at ~ 13 ppm is indicated in the insoluble products from 0.5 GPa, while
394 methyl groups were not detected (or are minimal) in the insoluble solid material formed at 1.5
395 GPa. These results imply that ring-opening reactions preferentially occur at lower pressure namely,
396 aromatic rings preferentially remained intact at higher pressure. Further experiments over a wider

range of pressures would be necessary to verify this possibility.

Conclusions

The self-condensation reaction of 1,5-Nap has been investigated at pressures of 0.5 and 1.5 GPa and temperatures ranging from 473 up to 623 K using a piston-cylinder-type high-pressure apparatus. The amount of recovery of unreacted 1,5-Nap significantly decreased in experiments run above 573 K at 0.5 GPa and above 623 K at 1.5GPa. Soluble reaction products were detected from >523K at 0.5 GPa and >548 K at 1.5 GPa, where the products of reaction include dimers, trimers and larger oligomers. Above 573 K at 0.5 GPa and above 598 K at 1.5 GPa, a black insoluble hydrogenated carbon nitride phase was obtained. IR spectra of both soluble and insoluble products suggested that the both products formed by a series of polymerization reactions. The present results indicated that polymerization progressed while maintaining N/C ratio of the 1,5-Nap reaction products in contrast that observed previously in 2,3-Nap, an isomer of 1,5-Nap where extensive N loss is observed [25]. Amongst the soluble products, three major types of the dimerization products were detected, these are products formed from naphthylation, exact dimerization, and dimerization with hydrogenation. Polymerization with naphthylation was also observed with pyrolysis of naphthalene [33, 43], even though the reaction temperature of 1,5-Nap was significantly lower than that observed in the aromatic hydrocarbon [33-34]. The presence of nitrogen atoms in the ring structure significantly lowered the temperature of the polymerization.

Polymerization with hydrogenation was observed with the reaction of 1,5-Nap, where such reactions has not been reported in pure aromatic hydrocarbons pyrolysis experiments [33, 43]. Whereas [2+2] and [4+2] Diels-Alder cycloaddition reactions are the likely initiation point to polymerization, subsequent dehydrogenation and hydrogenation reactions produces both dehydrogenated and hydrogenated dimers, the methine (CH) rich cyclo-addition products decompose to form predominantly bi-naphthyridine linkages eliminating H_2, thus the sp^3/sp^2 ratios and methine carbon content for the 1,5 Nap polymers are very low as compared with other pressure induced aromatic polymerizations. The major reaction mechanism of 1,5-Nap was similar at pressures of 0.5 and 1.5 GPa, although aromatic rings preferentially remained at the higher pressure.

Supplemental Information

See the supplemental information

Representative mass spectra of the soluble reaction products from the GC/MS analysis, ^{13}C ssNMR spectra of 1,5-Nap, fitting results of the ssNMR spectra from the insoluble products (spectra and a table), and a table for molar yield of the representative dimers.

Acknowledgements

We thank Dr. Oyama for assistance with the MALDI-TOF/MS measurements. A part of MALDI-TOF/MS measurements was performed at Faculty of advanced life science, Hokkaido University, registered in the Open Facility system managed by the Global Facility Center, Creative Research Institution, Hokkaido University. This work was supported by JSPS KAKENHI Grant Numbers 16K1783906 and 19K1480809, and by the Building of Consortia for the Development of Human Resources in Science and Technology, Ministry of Education, Culture, Sports, Science, and Technology, Japan. The solid-state NMR experiments were performed at the W. M. Keck Solid State NMR facility at the Earth and Planets Laboratory, which has received support from the Keck Foundation, the National Science Foundation, and the Carnegie Institution for Science.

444 **References**

445 1. Thomas, A.; Fischer, A.; Goettmann, F.; Antonietti, M.; Muller, J. O.; Schlogl, R.;

446 Carlsson, J. M., Graphitic Carbon Nitride Materials: Variation of Structure and Morphology and

447 Their Use as Metal-Free Catalysts. *J. Mater. Chem.* **2008**, *18*, 4893-4908.

448 2. Wang, X. C.; Maeda, K.; Thomas, A.; Takanabe, K.; Xin, G.; Carlsson, J. M.; Domen,

449 K.; Antonietti, M., A Metal-Free Polymeric Photocatalyst for Hydrogen Production from Water

450 under Visible Light. *Nat. Mat.* **2009**, *8*, 76-80.

451 3. Yan, S. C.; Li, Z. S.; Zou, Z. G., Photodegradation Performance of g-C_3N_4 Fabricated

452 by Directly Heating Melamine. *Langmuir* **2009**, *25*, 10397-10401.

453 4. Liu, A. Y.; Cohen, M. L., Prediction of New Low Compressibility Solids *Science* **1989**,

454 *245*, 841-842.

455 5. Liu, A. Y.; Wentzcovitch, R. M., Stabiliy of Carbon Nitride Solids. *Phy. Rev.B* **1994**, *50*,

456 10362-10365.

457 6. Teter, D. M.; Hemley, R. J., Low-Compressibility Carbon Nitrides. *Science* **1996**, *271*,

458 53-55.

459 7. Dong, H. F.; Oganov, A. R.; Zhu, Q.; Qian, G. R., The Phase Diagram and Hardness of

460 Carbon Nitrides. *Sci Rep* **2015**, *5*, 5.

461 8. Kroke, E.; Schwarz, M., Novel Group 14 Nitrides. *Coord. Chem. Rev.* **2004**, *248*, 493-

532.

9. Rodil, S. E.; Muhl, S., Bonding in Amorphous Carbon Nitride. *Diam. Relat. Mat.* **2004**, *13*, 1521-1531.

10. Miller, T. S.; Jorge, A. B.; Suter, T. M.; Sella, A.; Cora, F.; McMillan, P. F., Carbon Nitrides: Synthesis and Characterization of a New Class of Functional Materials. *Phys. Chem. Chem. Phys.* **2017**, *19*, 15613-15638.

11. Horvath-Bordon, E.; Riedel, R.; Zerr, A.; McMillan, P. F.; Auffermann, G.; Prots, Y.; Bronger, W.; Kniep, R.; Kroll, P., High-Pressure Chemistry of Nitride-Based Materials. *Chem. Soc. Rev.* **2006**, *35*, 987-1014.

12. Nesting, D. C.; Badding, J. V., High-Pressure Synthesis of sp^2-Bonded Carbon Nitrides. *Chem. Mat.* **1996**, *8*, 1535-1539.

13. Horvath-Bordon, E., et al., High-Pressure Synthesis of Crystalline Carbon Nitride Imide, $C_2N_2(NH)$. *Angew. Chem. Int. Edit.* **2007**, *46*, 1476-1480.

14. Kojima, Y.; Ohfuji, H., Structure and Stability of Carbon Nitride under High Pressure and High Temperature up to 125 GPa and 3000 K. *Diam. Relat. Mat.* **2013**, *39*, 1-7.

15. Alves, I.; Demazeau, G.; Tanguy, B.; Weill, F., On a New Model of the Graphitic Form of C_3N_4. *Solid State Commun.* **1999**, *109*, 697-701.

16. Zhang, Z. H.; Leinenweber, K.; Bauer, M.; Garvie, L. A. J.; McMillan, P. F.; Wolf, G.

480 H., High-Pressure Bulk Synthesis of Crystalline $C_6n_9h_3$ Center Dot Hcl: A Novel C_3N_4 Graphitic
481 Derivative. *J. Amer. Chem. Soc.* **2001**, *123*, 7788-7796.
482 17. Ma, H. A., et al., High-Pressure Pyrolysis Study of C_3n_6h6: A Route to Preparing Bulk
483 C_3N_4. *J. Phys. Condes. Matter* **2002**, *14*, 11269-11273.
484 18. Fang, L. M.; Ohfuji, H.; Shinmei, T.; Irifune, T., Experimental Study on the Stability of
485 Graphitic C_3N_4 under High Pressure and High Temperature. *Diam. Relat. Mat.* **2011**, *20*, 819-825.
486 19. Horibe, T.; Kusaba, K.; Niwa, K.; Hasegawa, M.; Yasuda, K.; Ishigami, R., Molecular
487 Routes Syntheses of Graphite-Like C-N Compounds with Various N/C Ratios in High Pressure
488 and Temperature. *J. Ceram. Soc. Jpn.* **2016**, *124*, 1013-1016.
489 20. Yasuzuka, T.; Komatsu, K.; Kagi, H., A Revisit to High-Pressure Transitions of Pyridine:
490 A New Phase Transition at 5 GPa and Formation of a Crystalline Phase over 20 Gpa. *Chem. Lett.*
491 **2011**, *40*, 733-735.
492 21. Fanetti, S.; Citroni, M.; Bini, R., Structure and Reactivity of Pyridine Crystal under
493 Pressure. *J. Chem. Phys.* **2011**, *134*, 204504.
494 22. Li, S. R., et al., Effect of Pressure on Heterocyclic Compounds: Pyrimidine and S-
495 Triazine. *J. Chem. Phys.* **2014**, *141*, 114902.
496 23. Citroni, M.; Fanetti, S.; Bini, R., Pressure and Laser-Induced Reactivity in Crystalline
497 S-Triazine. *J. Phys. Chem. C* **2014**, *118*, 10284-10290.

24. Yamane, I.; Yanase, T.; Nagahama, T.; Shimada, T., Search for New Nitrogen-Doped Carbon Materials by Compressing Molecular Crystals. *Jpn. J. Appl. Phys.* **2019**, *58*, 4.

25. Shinozaki, A.; Nagai, T.; Kagi, H.; Nakano, S., Pressure-Induced Irreversible Amorphization of Naphthalene and Nitrogen-Containing Heteroaromatic Compounds at Room Temperature. *Chem. Phys. Lett.* **2020**, *739*, 6.

26. Ciabini, L.; Santoro, M.; Gorelli, F. A.; Bini, R.; Schettino, V.; Raugei, S., Triggering Dynamics of the High-Pressure Benzene Amorphization. *Nat. Mat.* **2007**, *6*, 39-43.

27. Root, S.; Gupta, Y. M., Chemical Changes in Liquid Benzene Multiply Shock Compressed to 25 GPa. *J. Phys. Chem. A* **2009**, *113*, 1268-1277.

28. Li, X., et al., Carbon Nitride Nanothread Crystals Derived from Pyridine. *J. Ame. Chem. Soc.* **2018**, *140*, 4969-4972.

29. Fanetti, S.; Santoro, M.; Alabarse, F.; Enrico, B.; Bini, R., Modulating the H-Bond Strength by Varying the Temperature for the High Pressure Synthesis of Nitrogen Rich Carbon Nanothreads. *Nanoscale* **2020**, *12*, 5233-5242.

30. Fanetti, S.; Nobrega, M. M.; Teixeira-Neto, E.; Temperini, M. L. A.; Bini, R., Effect of Structural Anisotropy in High-Pressure Reaction of Aniline. *J. Phys. Chem. C* **2018**, *122*, 29158-29164.

31. Fitzgibbons, T. C.; Guthrie, M.; Xu, E-shi.; Crespi, V. H.; Davidowski, S. K.; Cody, G.

516 D.; Alem, N.; Badding, J. V., Benzene-Derived Carbon Nanothreads. *Nat. Mat.* **2015**, *14*, 43-47.

517 32. Li, X., et al., Mechanochemical Synthesis of Carbon Nanothread Single Crystals. *J. the*

518 *Ame. Chem. Soc.* **2017**, *139*, 16343-16349.

519 33. Chanyshev, A. D.; Litasov, K. D.; Furukawa, Y.; Kokh, K. A.; Shatskiy, A. F.,

520 Temperature-Induced Oligomerization of Polycyclic Aromatic Hydrocarbons at Ambient and

521 High Pressures. *Sci Rep* **2017**, *7*, 7889.

522 34. Chanyshev, A. D.; Litasov, K. D.; Shatskiy, A. F.; Furukawa, Y.; Yoshino, T.; Ohtani, E.,

523 Oligomerization and Carbonization of Polycyclic Aromatic Hydrocarbons at High Pressure and

524 Temperature. *Carbon* **2015**, *84*, 225-235.

525 35. Mimura, K.; Nishida, T., Hydrogen and Hydrocarbon Gases, Polycyclic Aromatic

526 Hydrocarbons, and Amorphous Carbon Produced by Multiple Shock Compression of Liquid

527 Benzene up to 27.4 GPa. *J. Phy. Chem. A* **2017**, *121*, 6471-6480.

528 36. Mimura, K.; Madono, T.; Toyama, S.; Sugitani, K.; Sugisaki, R.; Iwamatsu, S.; Murata,

529 S., Shock-Induced Pyrolysis of Naphthalene and Related Polycyclic Aromatic Hydrocarbons

530 (Anthracene, Pyrene, and Fluoranthene) at Pressures of 12-33.7 GPa. *J. Anal. Appl. Pyrolysis*

531 **2004**, *72*, 273-278.

532 37. Kondrin, M. V.; Nikolaev, N. A.; Boldyrev, K. N.; Shulga, Y. M.; Zibrov, I. P.; Brazhkin,

533 V. V., Bulk Graphanes Synthesized from Benzene and Pyridine. *Crystengcomm* **2017**, *19*, 958-

966.

38. Shinozaki, A.; Mimura, K.; Nishida, T., Decomposition and Oligomerization of 2,3-Naphthyridine under High- Pressure and High-Temperature Conditions. *Sci Rep* **2019**, *9*, 9.

39. Merritt, J. A.; Pirkle, R. J., Infrared and Raman Spectra of 1,5-Diazanapthalene *J. Mol. Spectrosc.* **1970**, *35*, 251-259.

40. Shinozaki, A.; Mimura, K.; Nishida, T.; Inoue, T.; Nakano, S.; Kagi, H., Stability and Partial Oligomerization of Naphthalene under High Pressure at Room Temperature. *Chem. Phys. Lett.* **2016**, *662*, 263-267.

41. Pretsch, E.; Buehlmann, P.; Affolter, C.; Pretsch, E.; Bhuhlmann, P.; Affolter, C., *Structure Determination of Organic Compound*; Springer: Berlin, 2000.

42. Robertson, J., Diamond-Like Amorphous Carbon. *Mater. Sci. Eng. R.* **2002**, *37*, 129-281.

43. Lewis, I. C., Thermal Polymerization of Aromatic Hydrocarbons. *Carbon* **1980**, *18*, 191-196.

44. Lewis, I. C., Chemistry of Carbonization *Carbon* **1982**, *20*, 519-529.

45. Shinozaki, A.; Mimura, K.; Kagi, H.; Komatu, K.; Noguchi, N.; Gotou, H., Pressure-Induced Oligomerization of Benzene at Room Temperature as a Precursory Reaction of Amorphization. *Jour. Chem. Phys.* **2014**, *141*, 084306.

552 46. Chanyshev, A. D., et al., High-Pressure-High-Temperature Study of Benzene: Refined
553 Crystal Structure and New Phase Diagram up to 8 GPa and 923 K. *Cryst. Growth Des.,* **2018**, *18*,
554 3016-3026.
555 47. Ciabini, L.; Gorelli, F. A.; Santoro, M.; Bini, R.; Schettino, V.; Mezouar, M., High-
556 Pressure and High-Temperature Equation of State and Phase Diagram of Solid Benzene. *Phys.*
557 *Rev. B* **2005**, *72*.
558 48. Fanetti, S.; Nobrega, M. M.; Dziubek, K.; Citroni, M.; Sella, A.; McMillan, P. F.;
559 Hanfland, M.; Bini, R., Structure and Reactivity of 2,4,6-Tricyano-1,3,5-Triazine under High-
560 Pressure Conditions. *Crystengcomm* **2019**, *21*, 4493-4500.
561 49. Chanyshev, A. D.; Litasov, K. D.; Shatskiy, A. F.; Sharygin, I. S.; Higo, Y.; Ohtani, E.,
562 Transition from Melting to Carbonization of Naphthalene, Anthracene, Pyrene and Coronene at
563 High Pressure. *Phys. Earth Planet. Inter.* **2017**, *270*, 29-39.
564

Figure captions

Figure 1 Molecular structure of 1,5-naphthyridine (1,5-Nap).

Figure 2 Temperature dependence of the residual ratio of 1,5-Nap at 0.5 GPa and 1.5 GPa (red and blue symbols, respectively), and that of naphthalene at 1.5 GPa 623 K (a black symbol).

Figure 3 Representative IR spectra of (a) starting material, (b) soluble products from 1.5 GPa, 623 K, (c) insoluble products from 1.5 GPa, 623 K, (d) insoluble products from 0.5 GPa, 623 K. Black dotted lines: The peaks observed in starting material. Red dotted lines: newly appeared in the reaction products. Str: stretching mode, Bend.: bending mode, Wag.: wagging mode, Def.: skeletal deformation mode

Figure 4 Representative TIC of GC/MS measurements after heating at (a) 623 K 1.5 GPa and (b) 573 K, 0.5 GPa. Numbers appeared with peaks represent the *m/z* of molecular ion peak. I.S. (1) and I.S. (2) are the methyl stearate and methyl triacontanoate, respectively used as internal standards. Mass spectra of (a)~(f) are shown in figure S1.

Figure 5 Molar yield of the reaction products (a) 0.5 GPa, (b) 1.5GPa. Residual ratio of 1,5-Nap is indicated above each bar. Relative molar yield of the reaction products for heating at (c) 0.5 GPa, (d) 1.5GPa.

Figure 6 MALDI-TOF/MS spectra of the recovered sample from 1.5 GPa, 573 K. The inset represents an enlarged view of the spectrum of 2 mers region at *m/z* = 250-290.

583 **Figure 7** ^{13}C CPMAS ssNMR of the insoluble products from 0.5 GPa, 623 K and 1.5 GPa, 623

584 K.

585 **Figure 8** (a) Possible dimerization pathways with [2+2] and [4+2] cycloaddition reactions. m.w.:

586 molecular weight. Possible linkages of the insoluble polymer with (b) [2+2] cycloaddition linkage,

587 (c) bi-naphthyridine linkage.

588

589 **Table 1** Experimental conditions of the present study.

no.	Staring material	Pressure (GPa)	Temperature (K)	Remaining 1,5-Nap (%)	Soluble products	Insoluble products
1	1,5-Nap	0.5	473	92.2	-	-
2	1,5-Nap	0.5	523	75.5	+	-
3	1,5-Nap	0.5	548	78.7	+	-
4	1,5-Nap	0.5	573	4.3	+	+
5	1,5-Nap	0.5	598	0.4	±	+
6	1,5-Nap	0.5	623	0.3	±	+
7	1,5-Nap	1.5	473	94.2	-	-
8	1,5-Nap	1.5	523	99.1	-	-
9	1,5-Nap	1.5	548	96.4	+	±
10	1,5-Nap	1.5	573	94.9	+	±
11	1,5-Nap	1.5	598	58.6	+	+
12	1,5-Nap	1.5	623	5.4	+	+
13	Nap	1.5	623	94.1	-	-

590 1,5-Nap: 1,5-naphthyridine, Nap: naphthalene, +: detected, - not detected, ±: trace amount

591

592 **TOC Graphic**

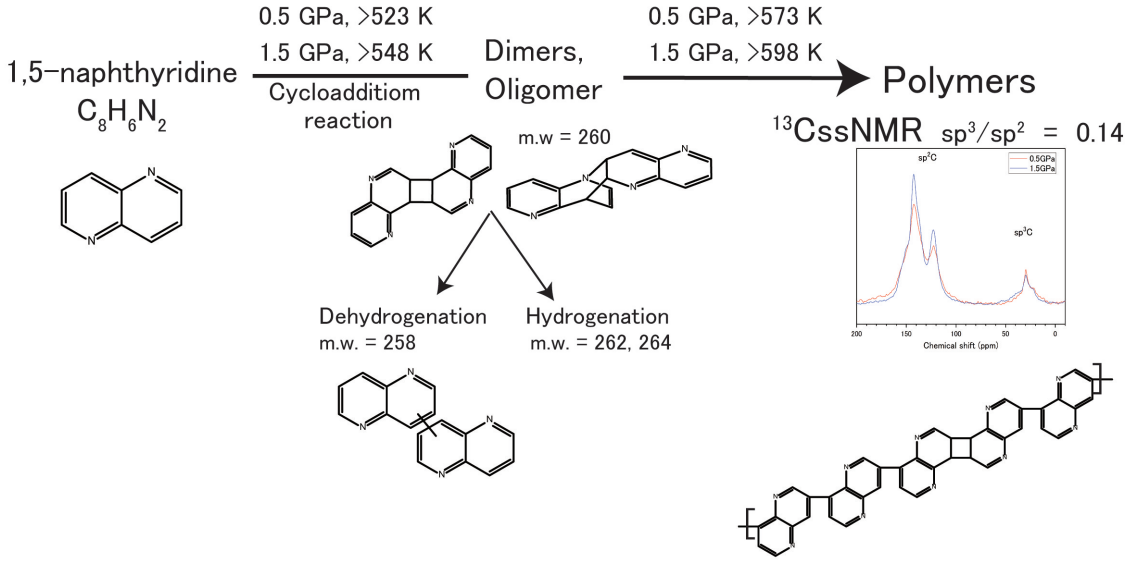

593

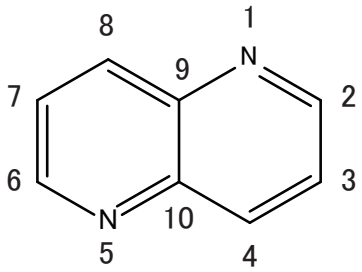

Figure 1

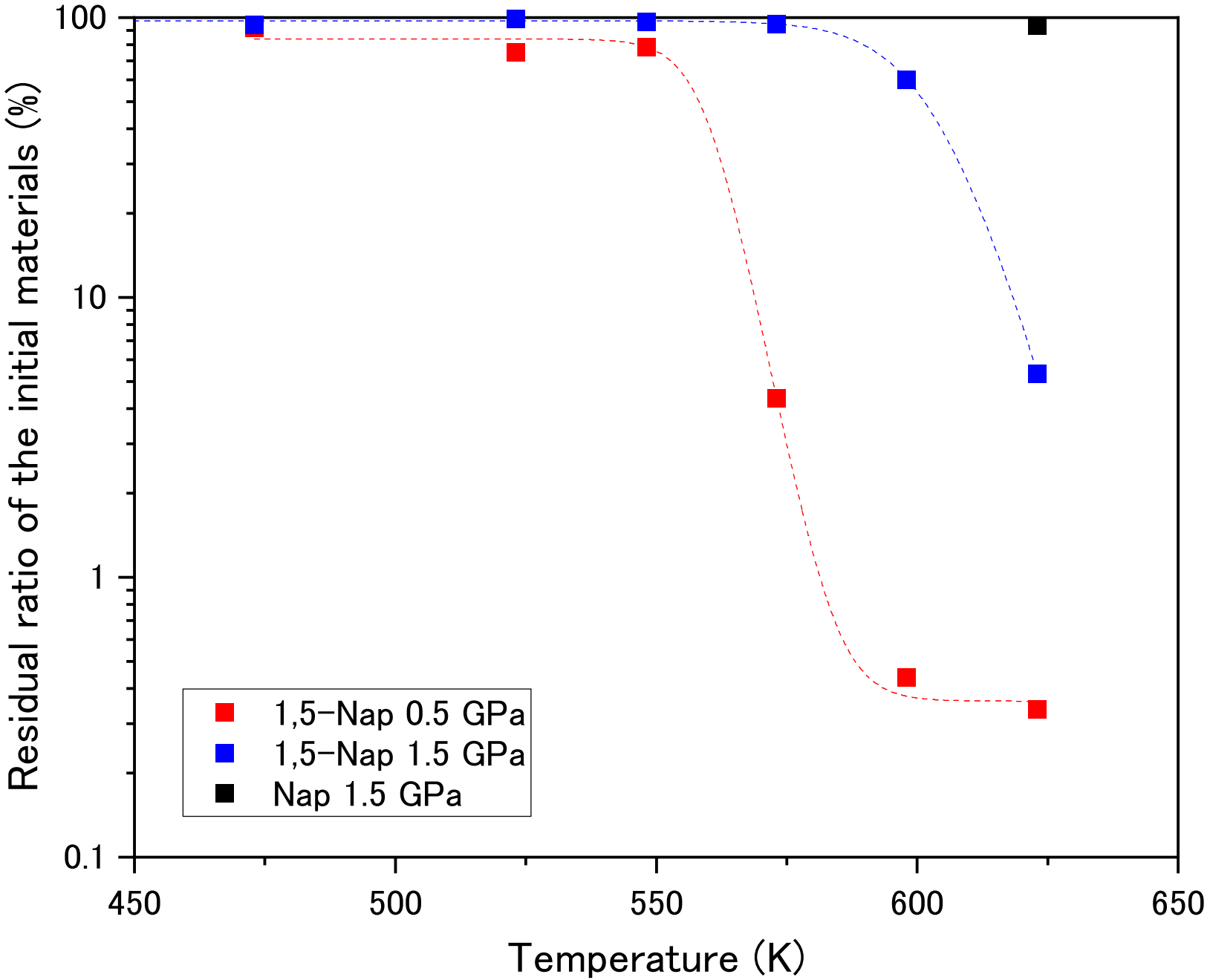
100
10
1
0.1
Residual ratio of the initial materials (%)
450
500
550
600
650
Temperature (K)
1,5-Nap 0.5 GPa
1,5-Nap 1.5 GPa
Nap 1.5 GPa

Figure 2

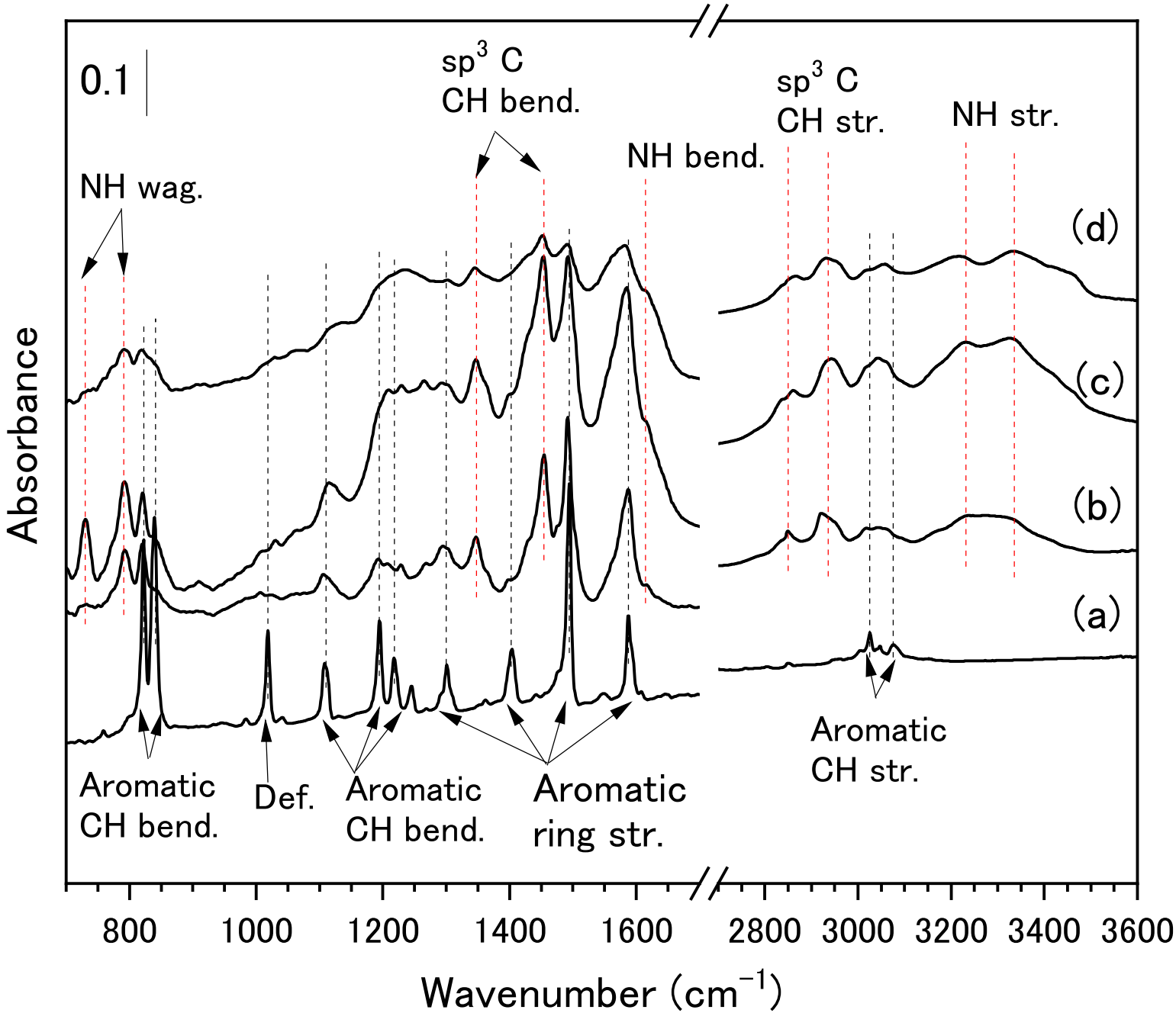
0.1
sp3 C
CH bend.
NH bend.
sp3 C
CH str.
NH str.
NH wag.
(d)
(c)
(b)
(a)
Absorbance
Aromatic
CH bend.
Def.
Aromatic
CH bend.
Aromatic
ring str.
Aromatic
CH str.
800
1000
1200
1400
1600
2800
3000
3200
3400
3600
Wavenumber (cm−1)

Figure 3

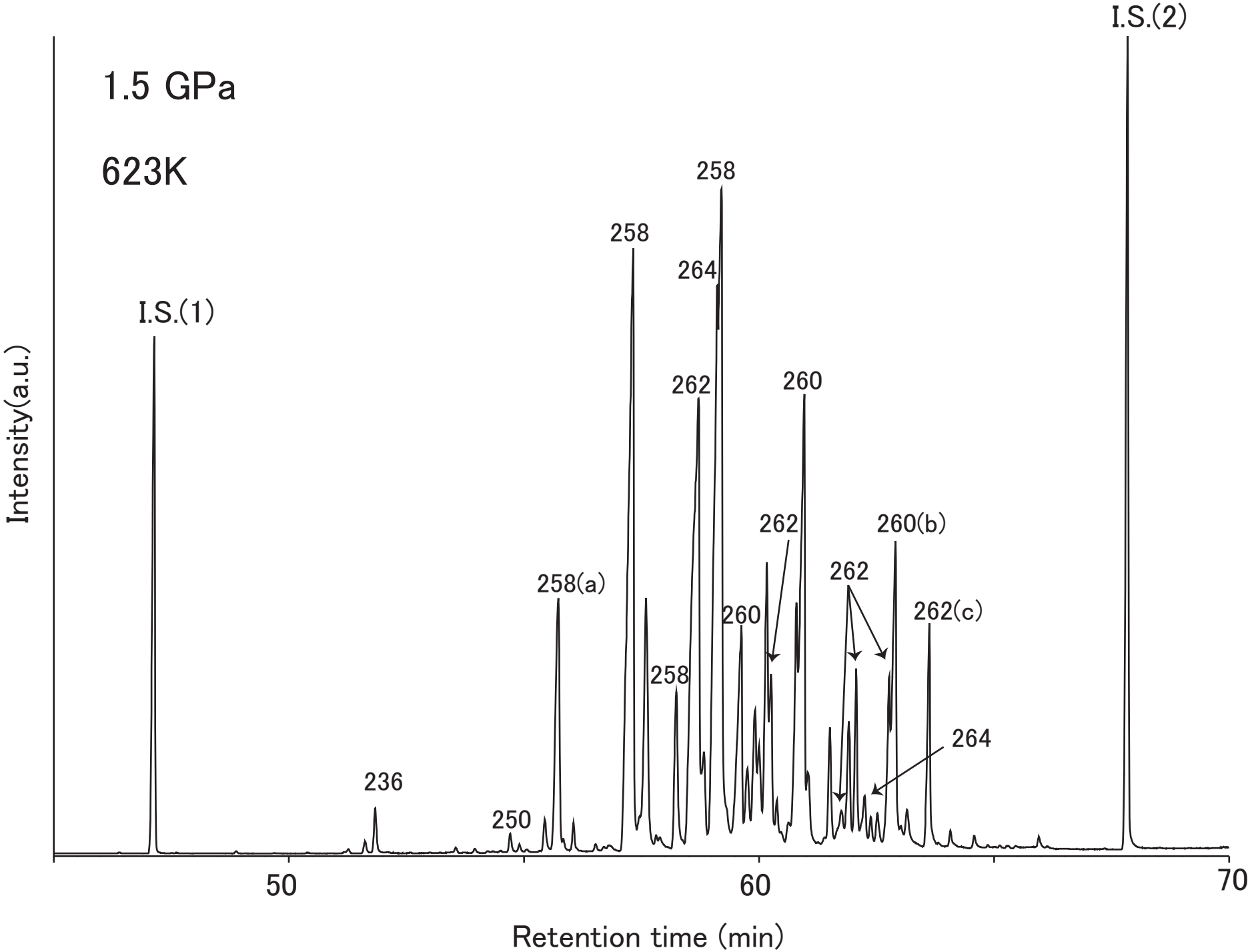
1.5 GPa
623K
I.S.(1)
I.S.(2)
258
258
264
262
260
262
260(b)
262
258(a)
260
262(c)
258
264
236
250
Intensity(a.u.)
50
60
70
Retention time (min)

Figure 4a

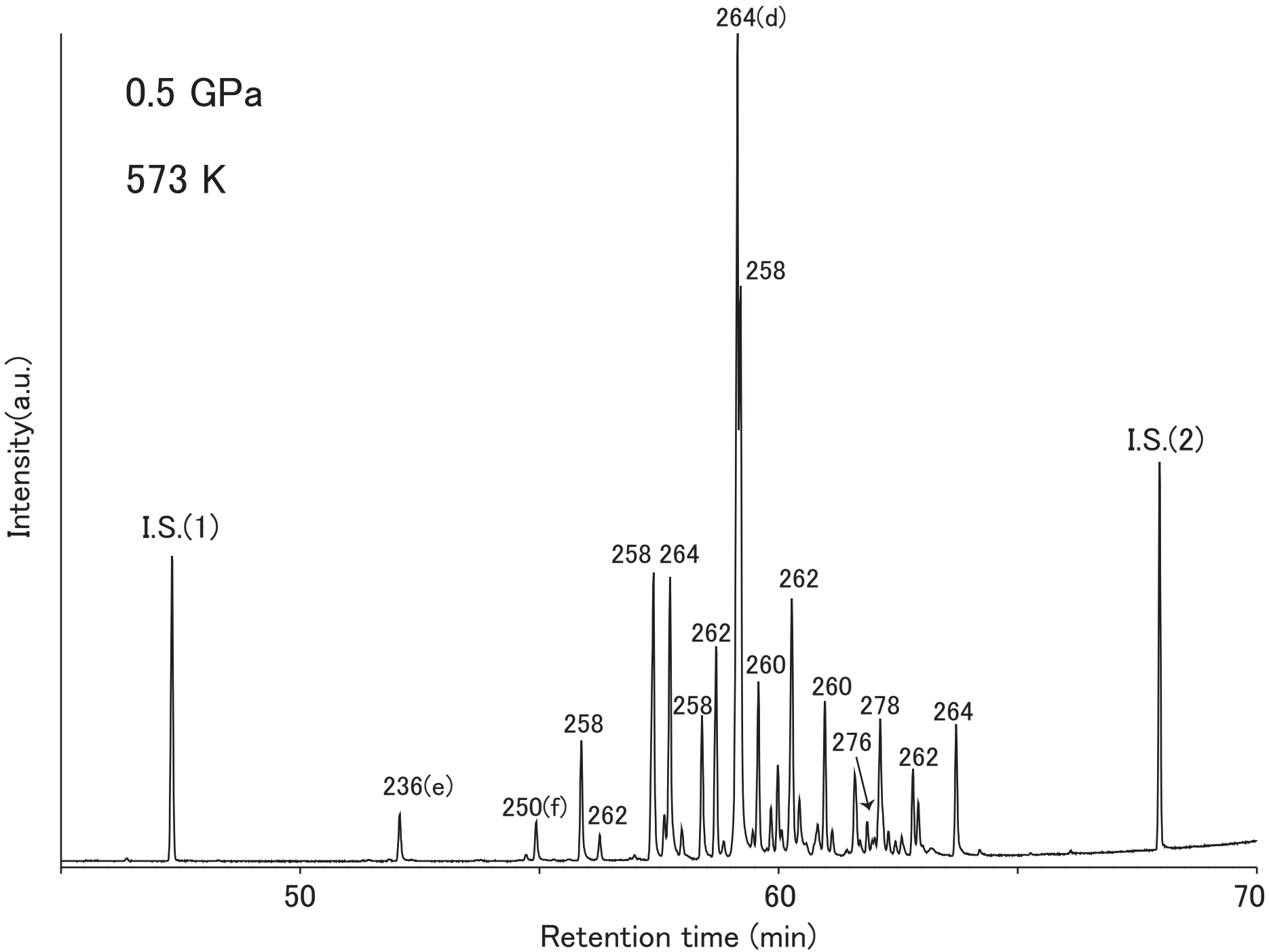
0.5 GPa
573 K
264(d)
258
I.S.(2)
I.S.(1)
258 264
262
262
260
260
278
264
258
276
262
258
236(e)
250(f)
262
Intensity(a.u.)
50
60
70
Retention time (min)

Figure 4b

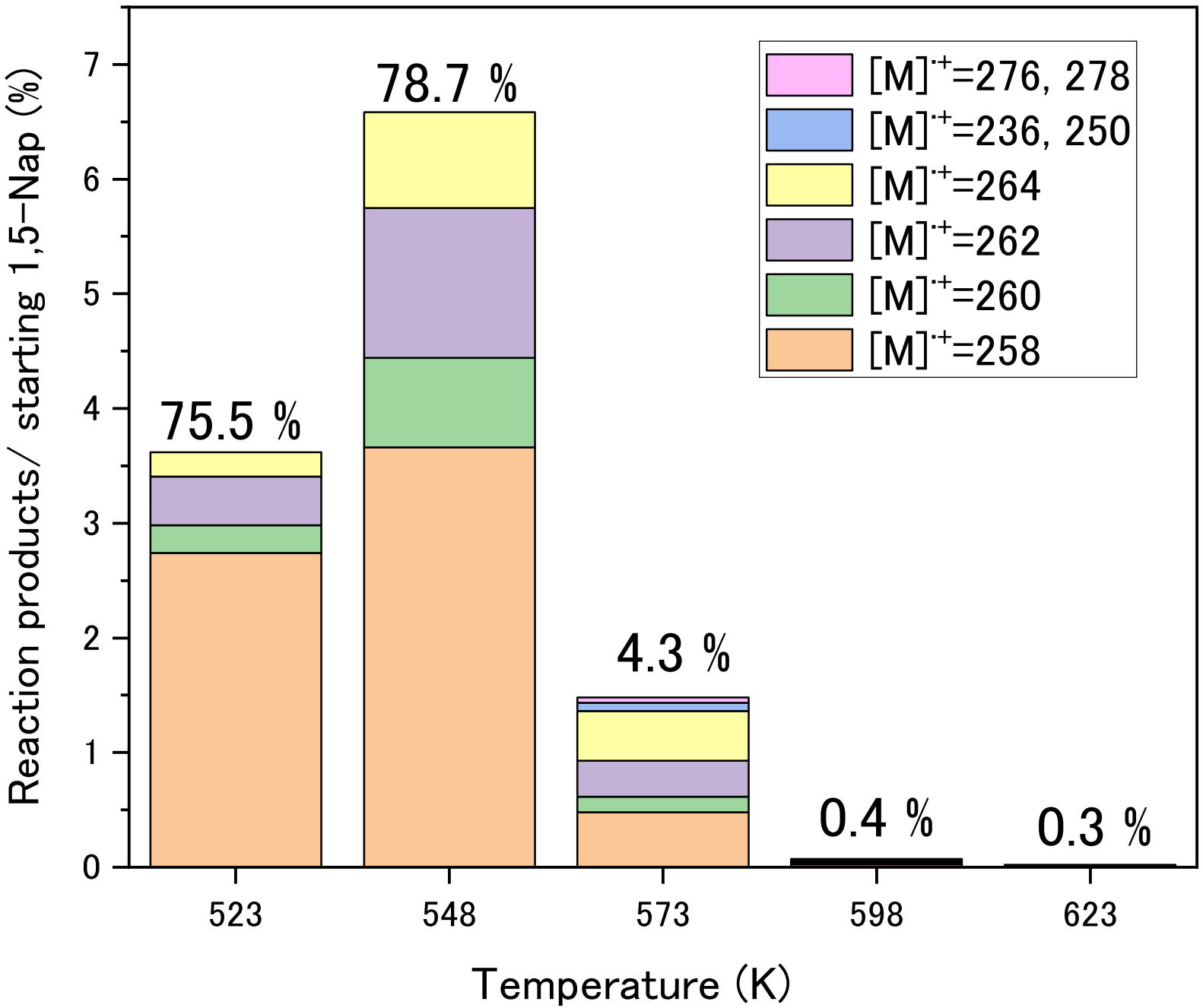
Reaction products/ starting 1,5-Nap (%)
0
1
2
3
4
5
6
7
523
548
573
598
623
Temperature (K)
75.5 %
78.7 %
4.3 %
0.4 %
0.3 %
[M]·+=276, 278
[M]·+=236, 250
[M]·+=264
[M]·+=262
[M]·+=260
[M]·+=258

Figure 5a

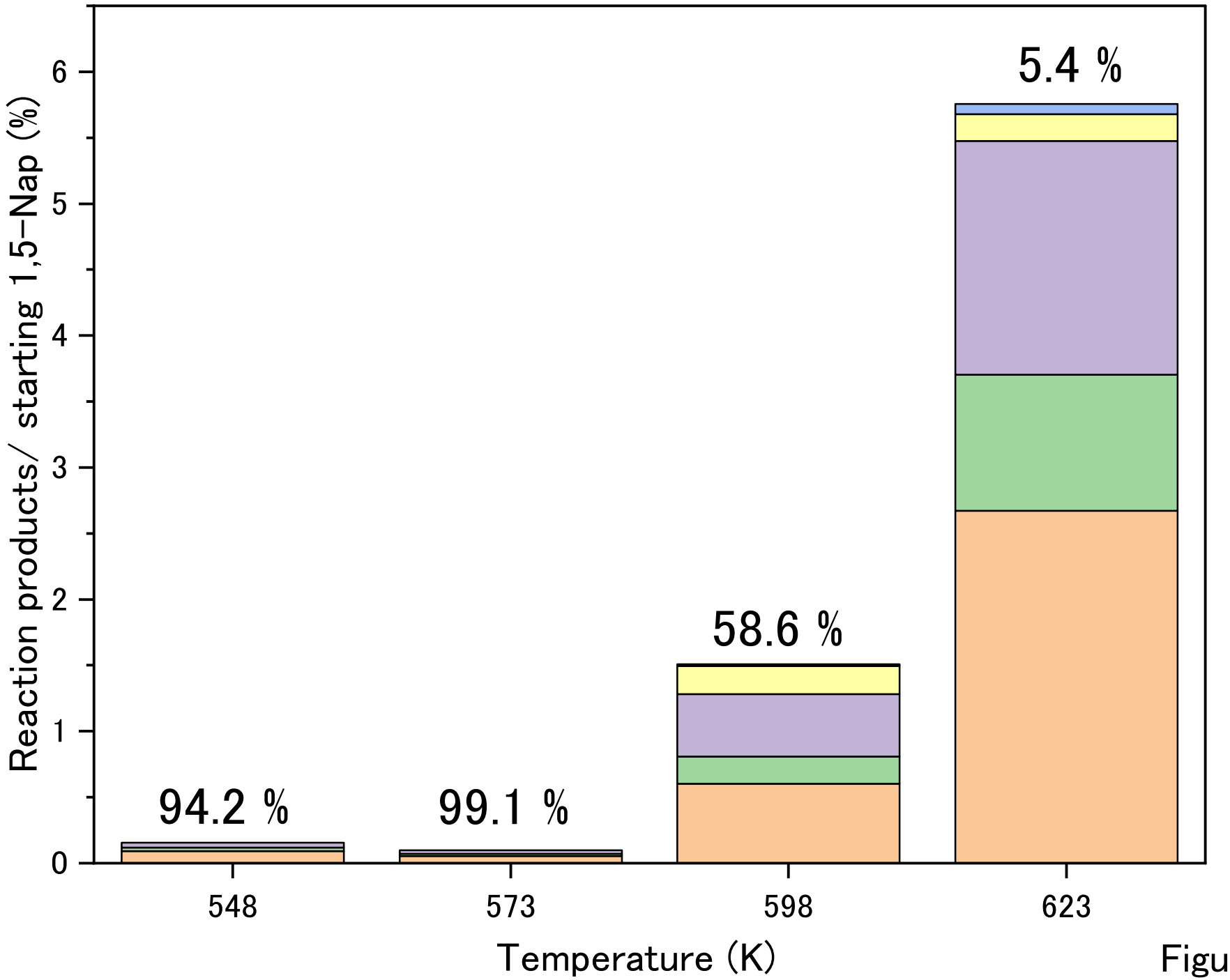
Reaction products/ starting 1,5-Nap (%)
0
1
2
3
4
5
6
94.2 %
99.1 %
58.6 %
5.4 %
548
573
598
623
Temperature (K)

Figure 5b

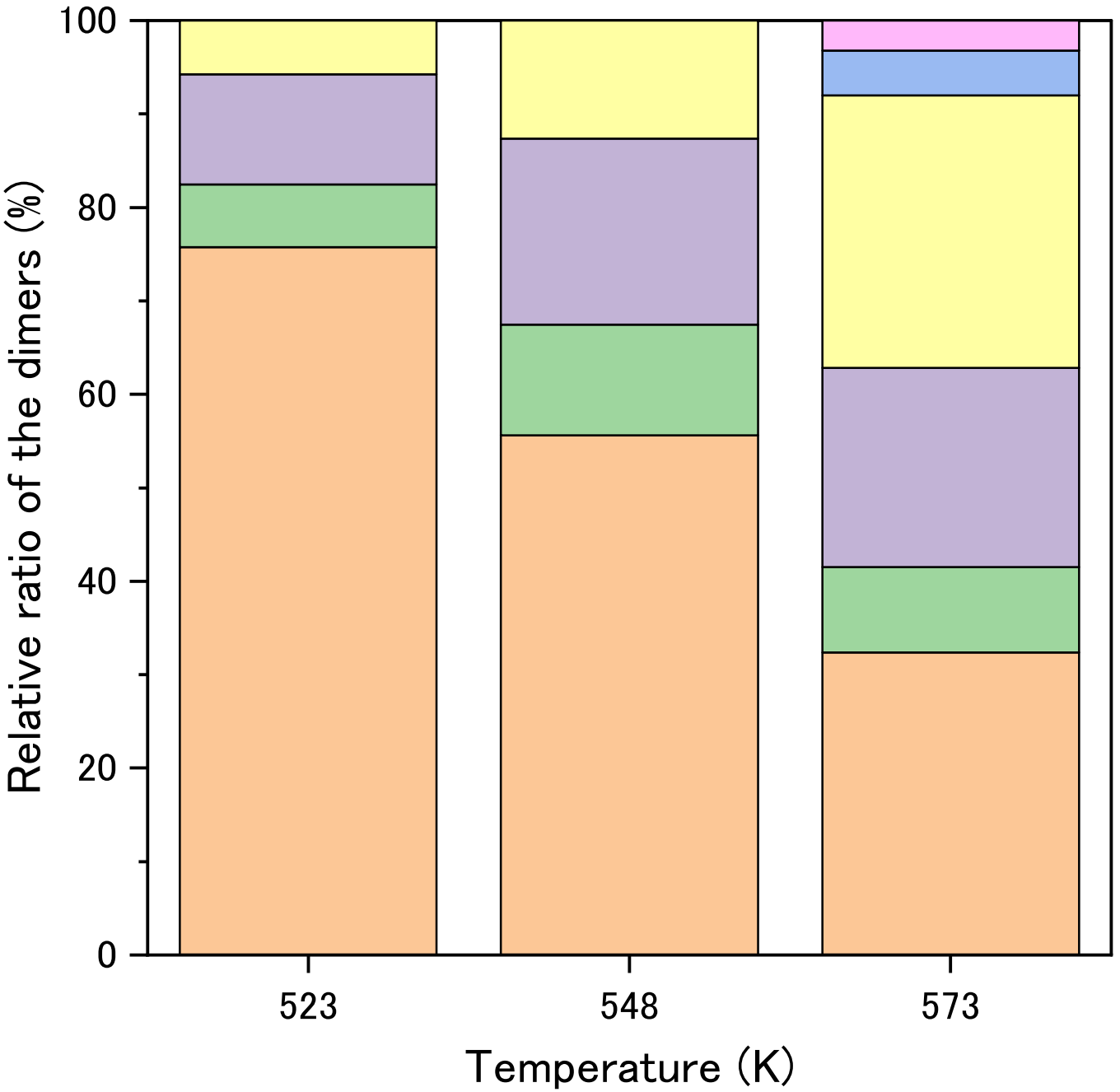
100
80
60
40
20
0
Relative ratio of the dimers (%)
523
548
573
Temperature (K)

Figure 5c

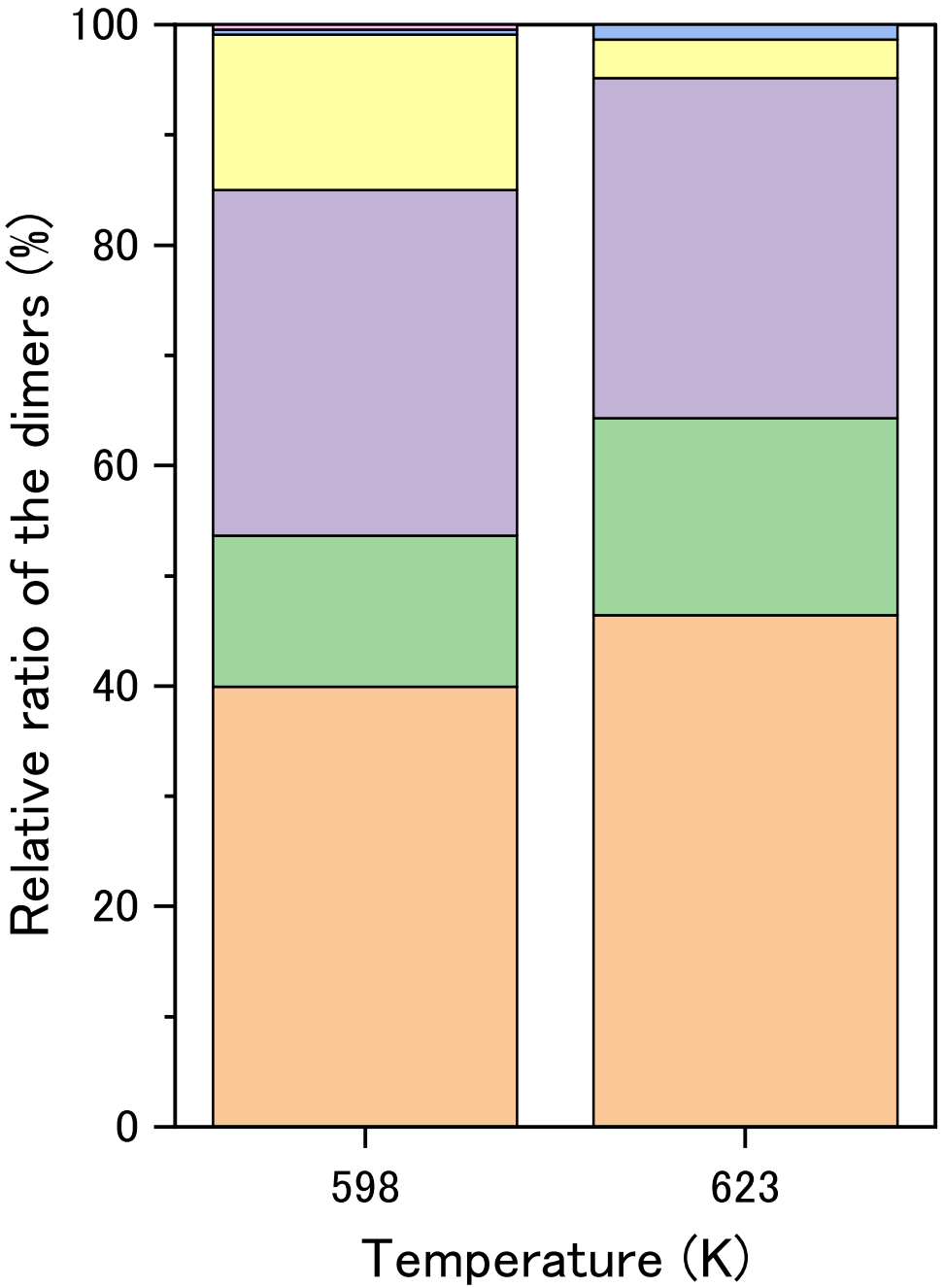
100
80
60
40
20
0
Relative ratio of the dimers (%)
598
623
Temperature (K)

Figure 5d

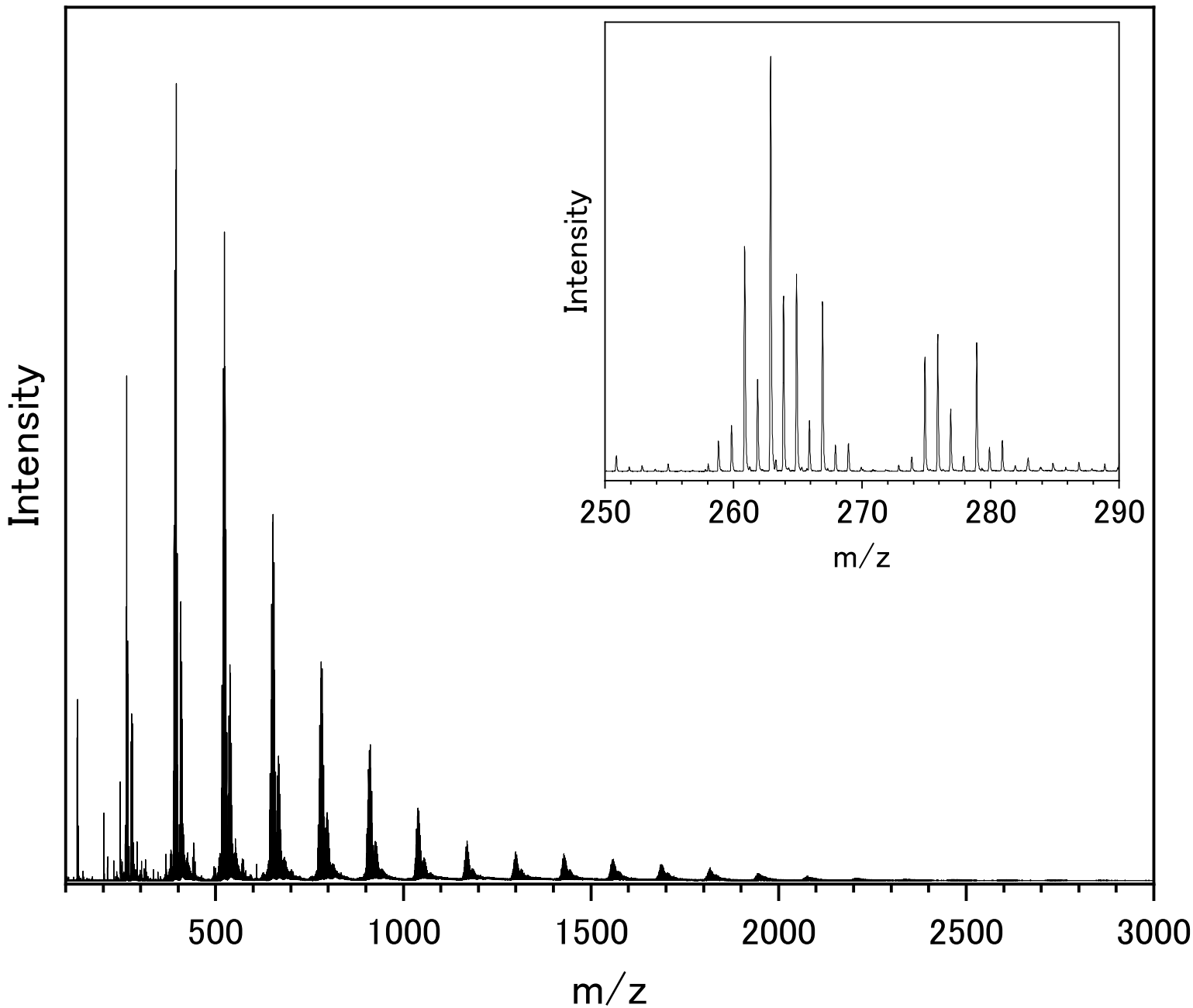
Intensity
500
1000
1500
2000
2500
3000
m/z
Intensity
250
260
270
280
290
m/z

Figure 6

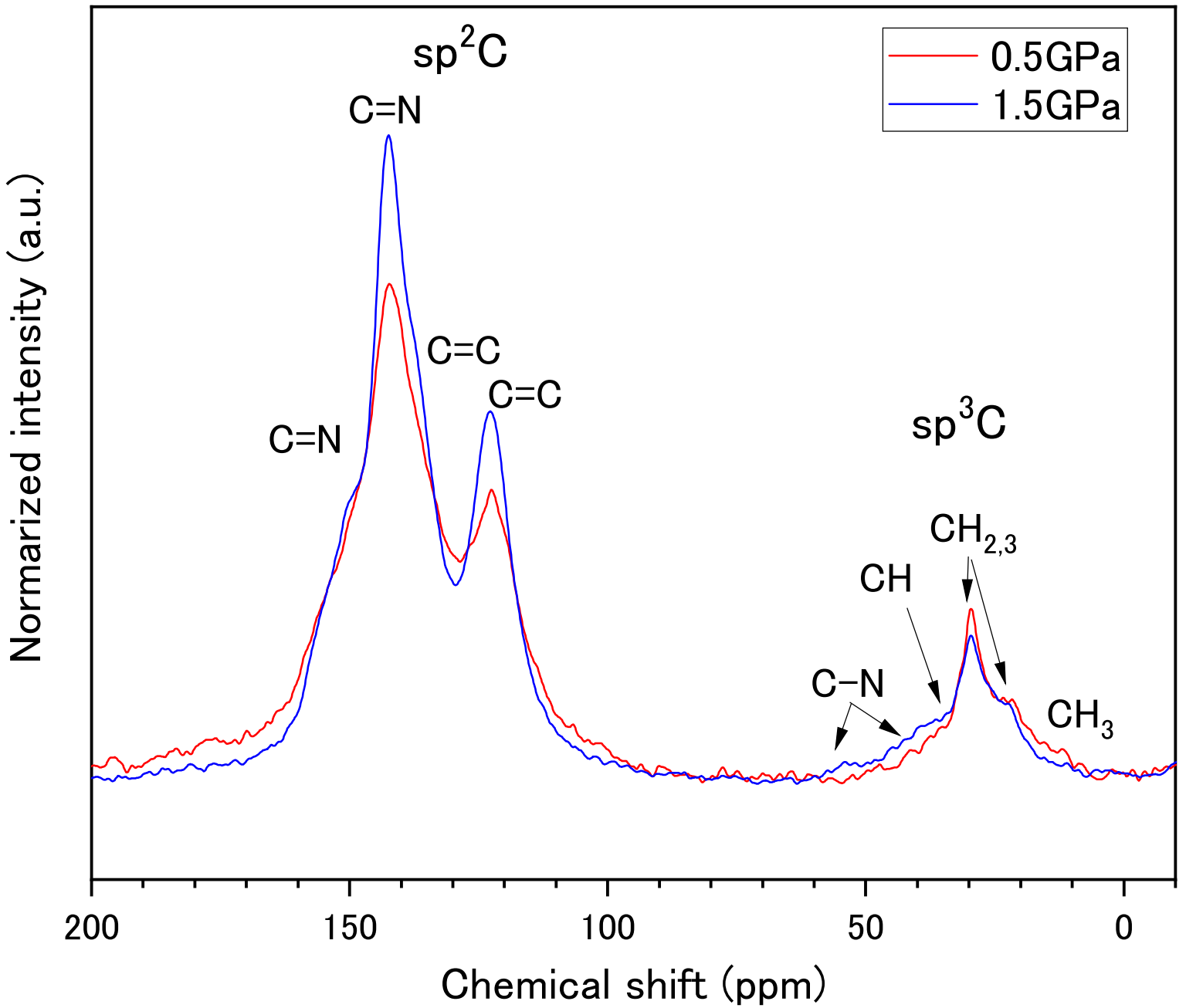
sp2C
C=N
C=C
C=C
C=N
sp3C
CH2,3
CH
C–N
CH3
0.5GPa
1.5GPa
Normarized intensity (a.u.)
200
150
100
50
0
Chemical shift (ppm)

Figure 7

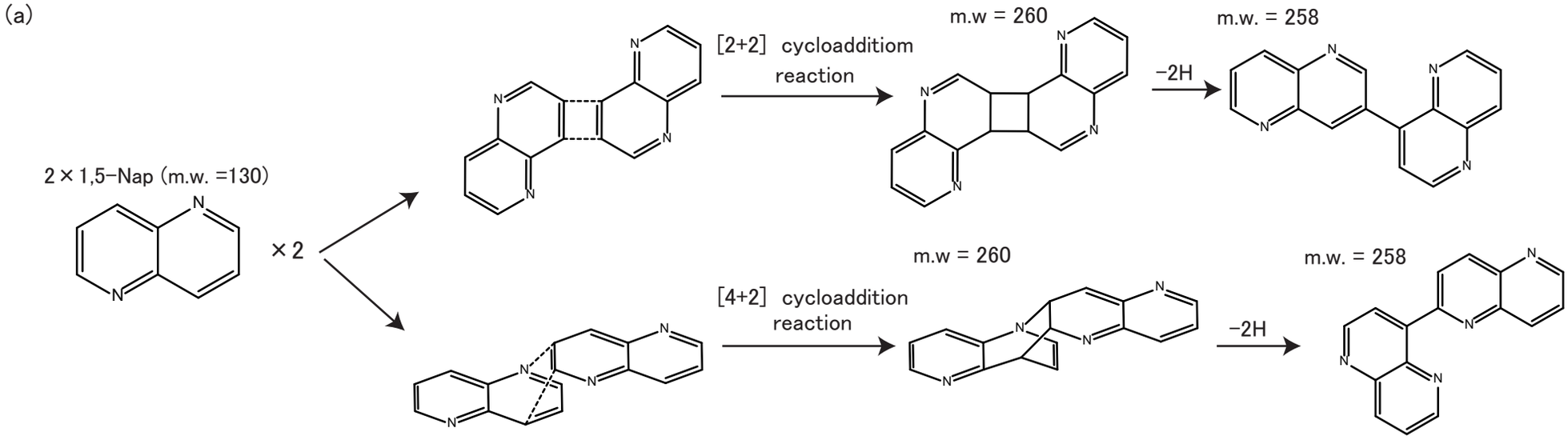
(a)
2 × 1,5-Nap (m.w. =130)
× 2
[2+2] cycloadditiom reaction
m.w = 260
−2H
m.w. = 258
[4+2] cycloaddition reaction
m.w = 260
−2H
m.w. = 258

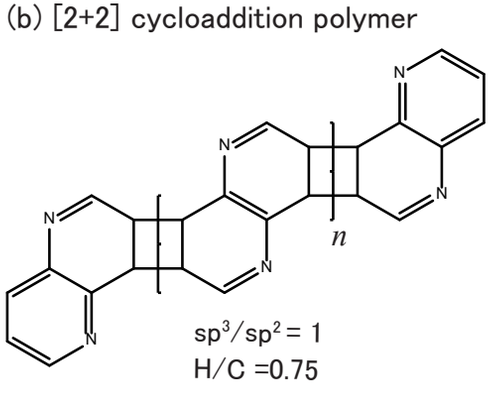
(b) [2+2] cycloaddition polymer
n
sp3/sp2 = 1
H/C =0.75

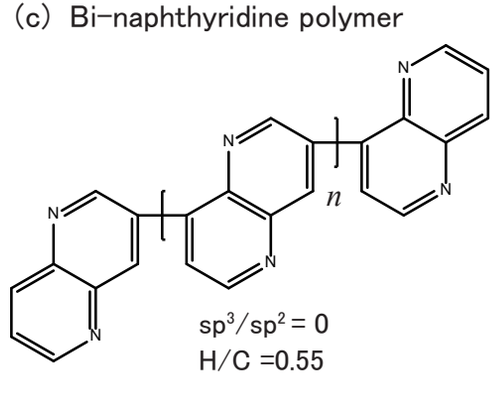
(c) Bi-naphthyridine polymer
n
sp3/sp2 = 0
H/C =0.55

Figure 8